AD-A110 745 ARCON CORP WALTHAM MA F/G 9/2
MATHEMATICAL ANALYSIS AND COMPUTER PROGRAM DEVELOPMENT FOR ELEC--ETC(U)
NOV 81 E TICHOVOLSKY, E COHEN, R SOLIN F19628-78-C-0202
UNCLASSIFIED RADC-TR-81-319 NL

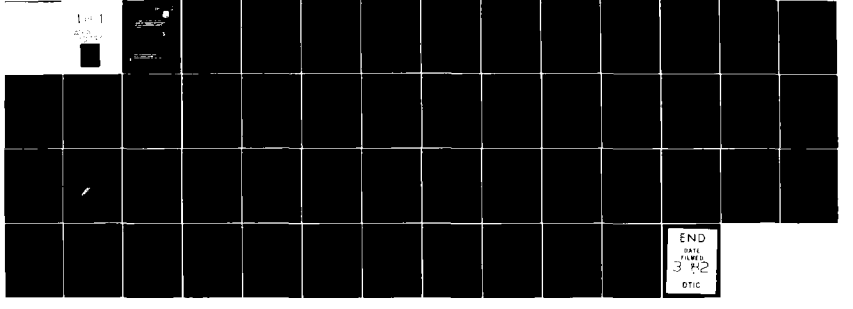

END
DATE FILMED
3 82
DTIC

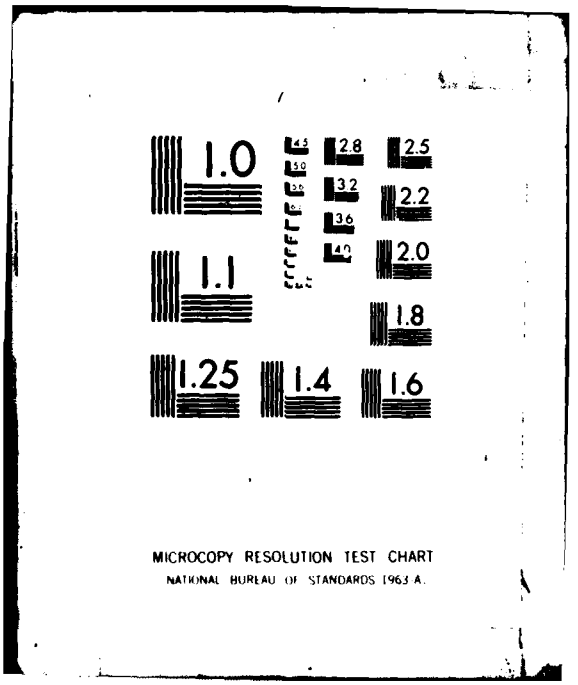
1.0
1.1
1.25
1.4
1.6
2.8
3.2
3.6
4.0
2.5
2.2
2.0
1.8
MICROCOPY RESOLUTION TEST CHART
NATIONAL BUREAU OF STANDARDS 1963 A.

This report has been reviewed and is approved for publication.

APPROVED: John P. Turtle

JOHN P. TURTLE
Project Engineer

APPROVED: Leo A. Whitcomb

LEO A. WHITCOMB, Chief
Electromagnetic Sciences Division

UNCLASSIFIED

SECURITY CLASSIFICATION OF THIS PAGE (When Data Entered)

REPORT DOCUMENTATION PAGE	READ INSTRUCTIONS BEFORE COMPLETING FORM
1. REPORT NUMBER: RADC-TR-81-319	2. GOVT ACCESSION NO.: AD-A110 745
	3. RECIPIENT'S CATALOG NUMBER:
4. TITLE (and Subtitle): MATHEMATICAL ANALYSIS AND COMPUTER PROGRAM DEVELOPMENT FOR ELECTROMAGNETIC SCIENCE STUDIES	5. TYPE OF REPORT & PERIOD COVERED: Final Technical Report Jul 78 - Jun 81
	6. PERFORMING ORG. REPORT NUMBER: N/A
7. AUTHOR(s): E. Tichovolsky, E. Cohen, R. Solin, T. Di-Beneditto, J. O'Brien, Y. Gersht, J. Bamforth, A. Weiss, N. Kerwin, Y. Krol, B. Blum	8. CONTRACT OR GRANT NUMBER(s): F19628-78-C-0202
9. PERFORMING ORGANIZATION NAME AND ADDRESS: ACRON Corporation, 260 Bear Hill Rd., Waltham MA 02154	10. PROGRAM ELEMENT, PROJECT, TASK AREA & WORK UNIT NUMBERS: 62702F, 9993MATH
11. CONTROLLING OFFICE NAME AND ADDRESS: Deputy for Electronic Technology (RADC/EEPL), Hanscom AFB MA 01731	12. REPORT DATE: November 1981
	13. NUMBER OF PAGES: 54
14. MONITORING AGENCY NAME & ADDRESS(if different from Controlling Office): Same	15. SECURITY CLASS. (of this report): UNCLASSIFIED
	15a. DECLASSIFICATION/DOWNGRADING SCHEDULE: N/A

16. DISTRIBUTION STATEMENT (of this Report)

Approved for public release; distribution unlimited.

17. DISTRIBUTION STATEMENT (of the abstract entered in Block 20, if different from Report)

Same

18. SUPPLEMENTARY NOTES

RADC Project Engineer: John P. Turtle (EEPL)

19. KEY WORDS (Continue on reverse side if necessary and identify by block number)

Electromagnetic Sciences
Antenna Theory
Acoustic Wave
Magnetostatic Wave
Very Low Frequency Propagation

20. ABSTRACT (Continue on reverse side if necessary and identify by block number)

This report contains representative examples of analysis and programming assignments executed for RADC technical personnel by staff of the ACRON Corporation. An assortment of analytical and computational problems as well as data processing tasks were performed relevant to Air Force projects requiring signal processing and electromagnetic theory. The core of the work pertained to LORAN-related studies, antenna theory, target detection and tracking problems, and the analysis of acoustic and magne-

DD FORM 1 JAN 73 1473 EDITION OF 1 NOV 65 IS OBSOLETE

UNCLASSIFIED

SECURITY CLASSIFICATION OF THIS PAGE (When Data Entered)

tostatic wave devices.

Table of Contents

Introduction

During the execution of contract 19628-78-C0202, ARCON staff worked with and provided computer software and analysis support for RADC technical personnel on numerous projects.

Most of the analysis and software development work involved the following topics: circular antenna array theory; detection and tracking of low flying targets by ground based radars; null-filter mobile radar software for a CSP-30 system; detection of a constant target in log-normal clutter; finite antenna subarrays irradiated with nonorthogonal illumination; calculations of field and radiation power patterns for a dipole array embedded in a wire mesh; radar data processing; simulation library for ground-based radars; analysis of single wire individual resource protection (WIRP) sensors; computation of received power from OTH radars; LORAN-related programs and problems; multi-hop propagation studies; modeling of VLF/LF propagations; whispering gallery theory; magnetostatic surface wave analysis, computations, and plotting; 3-D plotting VLF/LF ionosounding data; ducting in the ionosphere; ionogram construction; magnetic dipole radiation calculations; the analysis of bulk wave devices; and an assortment of related problems. Representative examples of the tasks performed will now be presented.

1. Sky-Wave Signal Analysis and Calculations

1.1 Introduction

Experimental methods for sounding the ionosphere have been described in considerable detail elsewhere. Ref. 1 provides an extensive list of such references. Of interest to us was the determination of the sky-wave return signal based on assumed models of the ionosphere and specification of a transmitted pulse. Because the models are often specified in the frequency domain, to obtain the sky-wave signal one is required to compute Fourier Transforms. Some of the special issues that arise with regard to reflection coefficient and full-wave models had to be taken into account as will become evident. Because of the amount of time required to perform the Fourier transforms using the classical computation approach, recourse to the Fast Fourier transform algorithm was deemed desirable.

1.2 Statement of the Problem

Under sufficiently quiescent conditions, it is reasonable to assume that the ionosphere does not significantly change its frequency-dependent propagation characteristics during one or more transmission-reception time frames. Apart from additive noise, one is justified in linearly relating the transmitted pulse, C(t), to the sky-wave return signal, o(t), through the convolution relationship

$$O(t) = C(t) \circledast h(t) \qquad (1)$$

h(t) corresponding to the impulse response of the ionosphere during the locally quiet period and $\circledast$ denoting aperiodic convolution.

With regard to ionospheric modelling, the evaluation of (1) is frequently of interest. We discuss the implementation of an off-the-shelf Fast Fourier transform (FFT) code to obtain o(t), and provide results based on an analytical expression for the frequency response of a slab ionosphere as well as data generated using a full-wave model.

Equation (1) can be expressed in the frequency domain as

$$o(t) = \int_{-\infty}^{\infty} \hat{C}(i\omega)\, \hat{H}(i\omega)\, e^{-i\omega t}\, d\omega \qquad (2)$$

where C and H are Fourier transforms of c(t) and h(t).
It is useful to partition the integration interval $(-\infty, \infty)$ into 3 regions:

$$\int_{-\infty}^{\infty} (\quad)\, d\omega = \int_{-\infty}^{-\omega_c} (\quad)\, d\omega + \int_{-\omega_c}^{\omega_c} (\quad)\, d\omega + \int_{\omega_c}^{\infty} (\quad)\, d\omega \qquad (3)$$

where

$$(\quad) = \hat{C}(i\omega)\, \hat{H}(i\omega)\, e^{-i\omega t}$$

If the product $\hat{C}(i\omega)\hat{H}(i\omega)$ vanishes outside some interval $(-\omega_c, \omega_c)$ the outer two integrals are zero. For the

time-limited functions c(t) and h(t), this is strictly not possible, but often the approximation is very good. The prolate spheroidal wavefunctions can be used as a basis if one is interested in confining, in some sense as "best as possible", functions both in the time and frequency domains to finite bands [Ref. 2]. But this was not considered necessary for the task requirements because the product $\hat{C}(i\omega)\hat{H}(i\omega)$ was nearly zero outside $(-\omega_c, \omega_c)$. The central problem was to develop a code for expeditiously computing

$$o(t) = \int_{-\omega_c}^{\omega_c} \hat{C}(i\omega)\ \hat{H}(i\omega)\, e^{-i\omega t}\, d\omega \qquad (4)$$

for various models of $\hat{H}(i\omega)$, the ionospheric transfer or frequency response function.

1.3 Numerical Fourier Transforms

Because $\hat{H}(i\omega)$ is often available as equispaced data samples, (4) was approximated with a weighted sum, i.e., quadrature expression. It should be noted that $\hat{C}(i\omega)\hat{H}(i\omega)$ is an aperiodic function in general. The standard procedure for constructing an equispaced quadrature approximation to (4) involving an aperiodic function is to sample ω uniformly:

$$\omega = \omega_n = n\,\frac{\omega_c}{N/2} \qquad \left(n = 0, \pm 1, \pm 2, \ldots, \pm \frac{N}{2}\right) \qquad (5)$$

It was further assumed that o(t) would be evaluated at uniformly spaced time intervals $t = t_m = m\,\Delta t$. It then follows that with quadrature weights , g_n,

$$O_m = O(t_m) = \int_{-\omega_c}^{\omega_c} \hat{C}(i\omega)\,\hat{H}(i\omega)\,e^{-i\omega t_m}\,d\omega \qquad (6)$$

$$\approx \Delta\omega \sum_{n=-\frac{N}{2}}^{\frac{N}{2}} g_n\,\hat{C}(i\omega_n)\,\hat{H}(i\omega_n)\,e^{-i\omega_n t_m} \qquad (7)$$

or in more convenient notation

$$O_m = \Delta\omega \sum_{n=-N/2}^{N/2} g_n\,\hat{C}_n\,\hat{H}_n\,e^{-i\frac{n\omega_c}{N/2}m\Delta t} \qquad (8)$$

The angular sampling frequency is now given by $\omega_s = 2\pi/\Delta t$, and must be consistent with the sampling theorems' requirement that $\omega_c \leq \omega_s/2$. For computational purposes, one can always choose a higher cut-off frequency $\omega_{c'}$, than the actual ω_c associated with the data, by filling samples in the range $\omega_c \leq \omega \leq \omega_{c'}$ with zeros. This is done so that

$$\omega_{c'}\,\Delta t = \frac{\omega_s}{2} \qquad (9)$$

Under these conditions, and setting

$$\hat{O}_n = g_n\,\hat{C}_n\,\hat{H}_n \qquad (10)$$

the quantity to be computed takes the form

$$O_m = \Delta\omega \sum_{n=-N/2}^{N/2} \hat{O}_n \exp[-2\pi i m n / N] \qquad (11)$$

Several problems arise using (11). It is easy to verify that $O_{m+\ell N} = O_m$ for $\ell = 0, \pm 1, \pm 2, \ldots$. By making use of discrete orthogonality, (11) can be inverted and also shows the periodic property that $\hat{O}_{n+pN} = \hat{O}_n$ for $p = 0, \pm 1, \pm 2, \ldots$. The original aperiodic functions $o(t)$ and $\hat{C}(i\omega)\hat{H}(i\omega)$ have now been transformed into periodic functions by virtue of the complex exponentials and equispaced sampling in both domains. Furthermore, whereas the original aperiodic functions correspond to different frequency or time samples throughout their ranges, the induced periodicity of O_m and $\hat{O}_n$ creates a discontinuity at their endpoints $m\,(\text{or } n) = \pm N/2$: the points $m\,(\text{or } n) = \pm N/2$ do not correspond to distinct times or frequencies because

$$e^{-2\pi i m (\pm N/2)} = (-1)^m \qquad (12)$$

is independent of sign. Fig. 1 depicts the situation. Because of the periodic replication of the original function, there will be discontinuities at

$$m \ (\text{or } n) = \pm \frac{N}{2} + \ell N \qquad (\ell = 0, \pm 1, \pm 2, \ldots)$$

In general, then, there can be discontinuities in the function values and derivatives at the endpoints. With a function discontinuity in $\hat{O}(i\omega)$, there will be a corresponding component in the time domain function that will fall off very slowly; namely, as 1/m. To remedy this, one can initially subtract off a linear

component from $\hat{O}(i\omega)$ and treat its finite Fourier transform separately and analytically [Ref. 3]. The remainder function will then fall off at least as fast as $1/m$, and can be treated numerically using an FFT implementation of a DFT. Other methods are also available to handle endpoint corrections for step, slope or higher order discontinuites [Ref. 3]. They were judged unnecessary in our efforts because it was found that for the data being considered

$$|\hat{O}|_{\omega=\pm\omega_c} \approx 0 \quad \text{and} \quad \frac{d}{d\omega}|\hat{O}|_{\omega=\omega_c} \approx 0$$

To avoid counting the endpoint contribution at N/2 twice, resulting from the periodic replication, one can set $\hat{O}_{\frac{N}{2}} = 0$ or assign a weight of 1/2 to both $\hat{O}_{N/2}$ and $\hat{O}_{-N/2}$. See Harris [Ref. 4]. For the former, this leads to the discrete Fourier transform (DFT) expression

$$O_m = \Delta\omega \sum_{n=-N/2}^{N/2} \hat{O}_n \exp[-2\pi i\, mn/N] \tag{13}$$

It is often more convenient to make use of the periodicity and use a different range of m and n; viz.,

$$O_m = \Delta\omega \sum_{n=0}^{N-1} \hat{O}_n \exp[-2\pi i\, mn/N] \tag{14}$$

As shown in Fig. 2 for the interval $[0, N-1]$, the range

$[0, \frac{N}{2}-1]$ corresponds to ω or $t \geq 0$, while the range $[\frac{N}{2}, N-1]$ corresponds to ω or $t < 0$. An FFT is particularly convenient to use for the determination of O_m when N > 128. Using 1024 complex samples in much of our work, the time required to compute an FFT was found to be less than 0.15 seconds using the CDC-6600 computer.

In the numerical Fourier transform program that was tailored to sky-wave data, most of the time required to obtain O_m went into "overhead" operations: Construction of the functions that comprise $\hat{O}_n$, choosing particular program options, putting the data into arrays of special lengths, windowing various functions, etc. Under these conditions, to obtain O_m using a string of full-wave data for $\hat{H}(i\omega)$ and a given c(t) pulse took about 6 seconds of CP time. By way of comparison, it is interesting to note that direct evaluation at only 13 time points of h(t) for 2000 samples of $\hat{H}(i\omega)$ required about 26 seconds of execution time, whereas using an FFT on 2048 samples of $\hat{H}(i\omega)$ gave all 2048 samples of h(t) while requiring about 2.3 seconds of execution time.

1.4 Fast Convolution

A fast convolution code for continuous-time functions was written and tested on cases that could be evaluated in closed form. A standard method for effecting the convolution was adopted and will now be summarized. Variations of it appear in the literature and depend primarily on accuracy and speed requirements, as well as the class of functions involved. The procedure we adopted was the following:

1. The sampled input time signal, C_n, is quadrature weighted using the factors g_n.

2. The DFT of $g_n C_n$ is computed using an FFT code.

3. The frequency response or transfer function of the sys-

tem (i.e., ionosphere) is specified either from a tape file or formulas evaluated within the program.

4. The product of the transformed input signal and frequency response is computed.

5. The product is smoothed using Lanczos σ-factors, and the inverse DFT is computed to give the output signal.

The achieve aperiodic convolution, the duration of the C(t) pulse and the effective duration of the impulse response of the system must be less than 1/2 the number of DFT sample points times the sampling interval, Δt . If this condition is not met, the output signal is not convolved aperiodically [See Oppenheim and Schaffer, Ref. 5]. To insure that this was met, the impulse response, h(t), was usually computed first with a numerical Fourier transform code and examined. This provided us with information relevant to the effective time duration of the impulse response function.

For discrete functions the σ-factors take the form

$$\left.\begin{aligned} \sigma_i &= \sin\left(\tfrac{2\pi}{L}\right)i \Big/ \left(\tfrac{2\pi}{L}\right)i \\ \sigma_{L-i} &= \sigma_i \end{aligned}\right\} \; i = 1, 2, \ldots, \tfrac{L}{2}-1 \qquad (15)$$

$$\sigma_{\frac{L}{2}} = \sigma_{\frac{L}{2}-1} = 0.$$

$$\sigma_0 = 1.$$

remembering that for an L-point DFT, the samples indexed by $L/2 < i < L$ corresponds to the negative frequency (or time) region. The use of σ-factors is usually employed for finite Fourier series, for discrete or continuous functions, especially if the transformed function is suspected of exhibiting strong Gibb's phenomena, which was the case when a slab ionosphere model was used. See Appendix I. The impulse response for the ionosphere in this situation was observed to have a "switch-like" behavior, being "switched on" for about 50 microseconds and off thereafter. The pulse or switch behavior was quite noticable for normal incidence to the slab ionosphere. Using the σ-factors, severe ringing effects were suppressed, accompanied by negligible pulse broadening.

As an alternative means for suppressing ringing and ripples, a 4-term Blackman-Harris window was also tried. While it greatly suppressed the out-of-band ripples in the pulse-like h(t) function, it was at the expense of considerable broadening and distorting of the pulse. The Blackman-Harris window coefficients had been obtained from a paper by Harris [Ref. 4], and the weights were good to only 5 significant digits. This created accuracy problems when the number of DFT samples was increased above 1024. In the end, this particular filter was eliminated from out work.

Because of the nonrecursive filtering methods adopted in our investigations, the broadening of the pulse, h(t), makes it appear as if the ionosphere begins to respond prior to $t = 0$. This, of course, is not the case; rather, the non-causal appearance is due to the limitations of the mathematics in the vicinity of the sudden response at t=0.

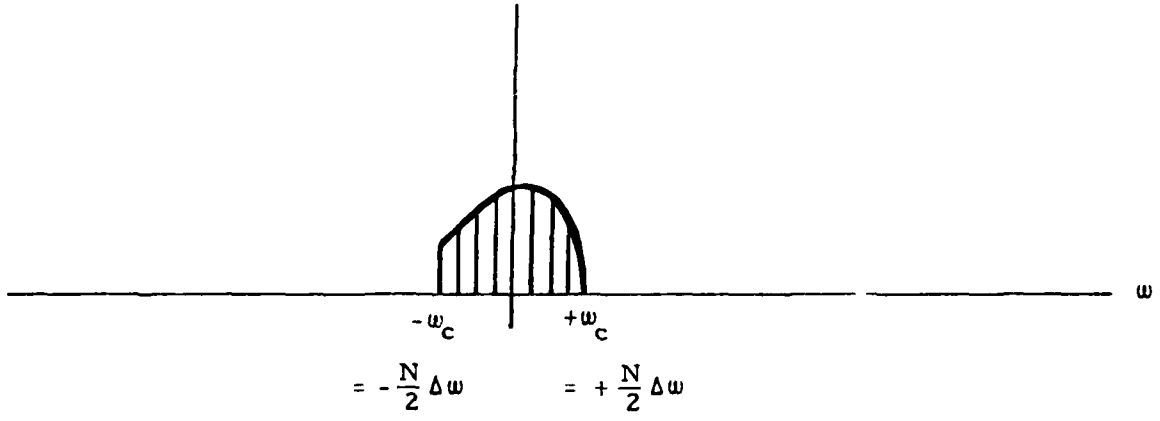

Original Aperiodic Function, Sampled

Figure 1a

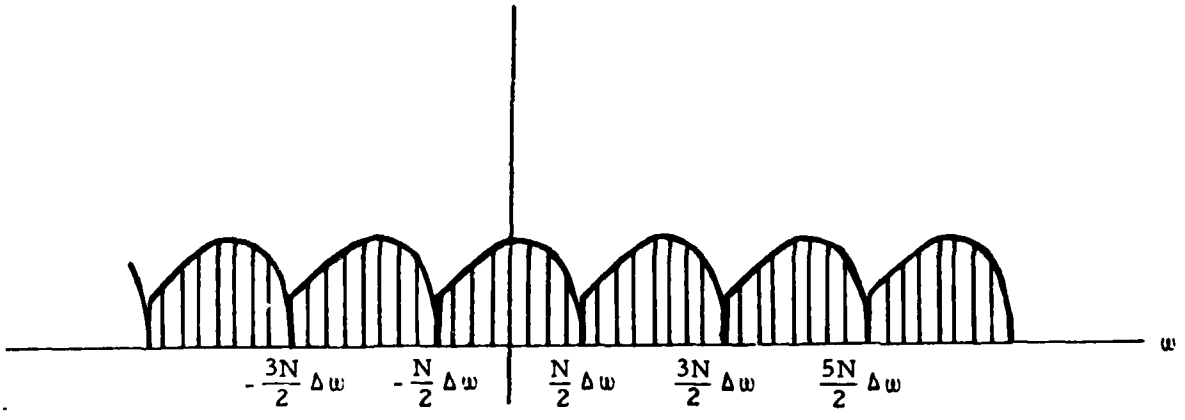

Periodic Replication Induced by DFT
of Original, Sampled Function

Figure 1b

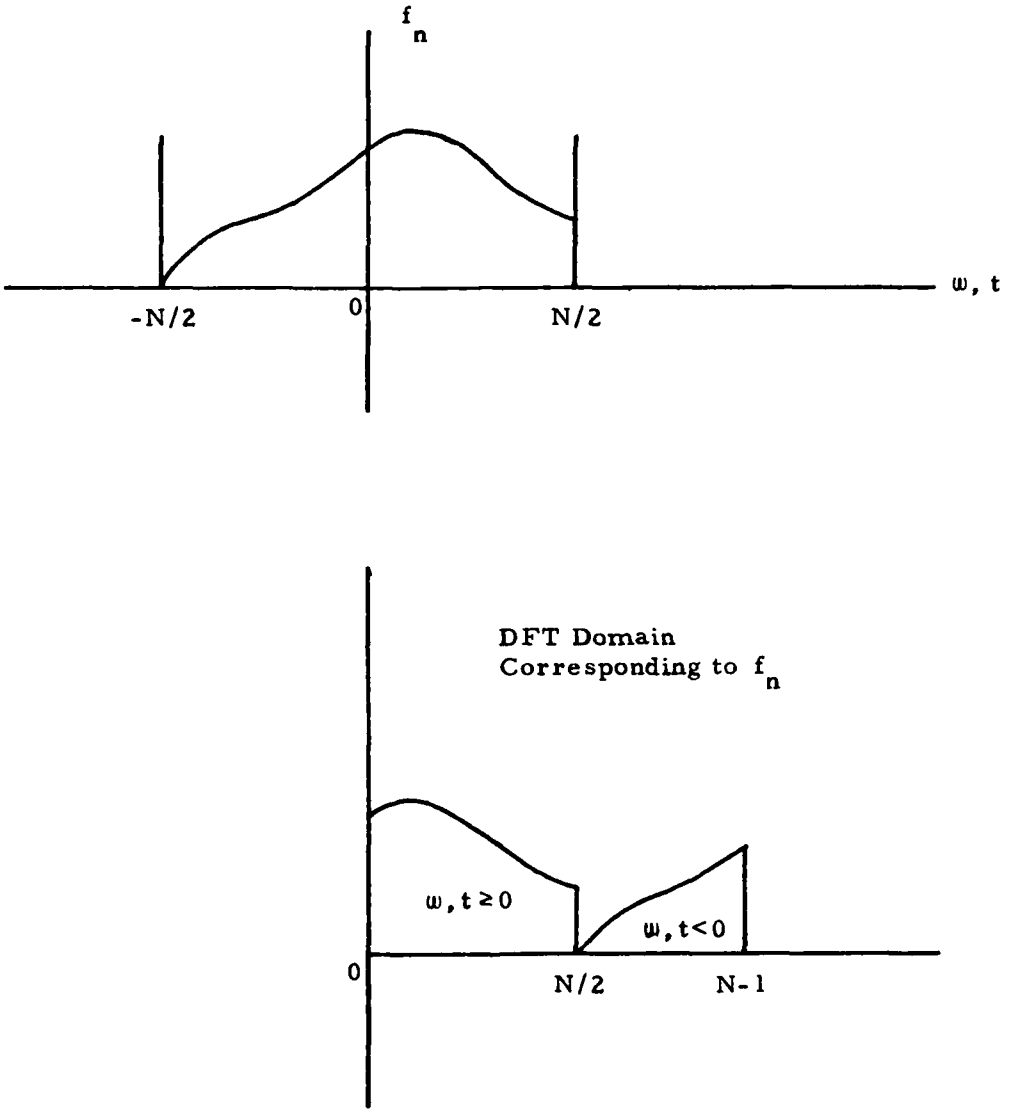

Domains for Time, Frequency, and DFT Samples

Figure 2

APPENDIX I

$R_{TM}(i\omega)$ - Slab Ionosphere Model

For the slab ionosphere, the frequency-dependent reflectivity for TM radiation is of the following form:

$$R_{TM}(i\omega) = \frac{Q(i\omega)\left[1 - e^{i2KL\cos\theta}\right]}{1 - Q^2(i\omega)\, e^{i2KL\cos\theta}} \qquad \text{(A-1)}$$

where

$$Q(i\omega) = \frac{-\left[1 + \frac{i\sigma}{\omega\epsilon_0\cos^2\theta}\right]^{1/2} + \left[1 + \frac{i\sigma}{\omega\epsilon_0}\right]}{\left[1 + \frac{i\sigma}{\omega\epsilon_0\cos^2\theta}\right]^{1/2} + \left[1 + \frac{i\sigma}{\omega\epsilon_0}\right]} \qquad \text{(A-2)}$$

$$K = K_0\left[1 + i\sigma/(\omega\epsilon_0\cos^2\theta)\right]^{1/2}$$

$K_0 = 2\pi f/c = \omega/c$

σ = conductivity e.g. 2.E-9 mhos/m

L = slab ionosphere thickness e.g. 7.5 km

$\epsilon_0 = 1.E-9/36\pi$

θ = angle of incidence

To avoid the "apparent" singularity at $\omega = 0$, $R_{TM}(0)$ was evaluated numerically at $\omega = 0^{+} \equiv 1.E-9$. Using R_{TM} as the frequency-response of the ionosphere, the impulse response was then determined through a numerical Fourier transform computation.

REFERENCES

1. Rasmussen, Kossey, and Lewis, "Evidence of an Ionosphere Reflecting Layer Below the Classical D Region", Journal of Geophysical Research, Vol. 85, No. A6, pp. 3037, June 1980. (See the references at the end of the paper.)

2. Papoulis, Signal Analysis, Chapter 6, 1977.

3. Lanczos, Applied Analysis, pp. 331-336, 1964.

4. Harris, "On the Use of Windows for Harmonic Analysis with the Discrete Fourier Transform", Proc. of IEEE, Vol. 66, No. 1, January 1978, pp. 51-83.

5. Oppenheim and Schaffer, Digital Signal Processing, Prentice-Hall, New Jersey, 1975.

2. Bulk Wave Investigations

2.1 SSBW Transducers

Surface-skimming bulk wave (SSBW) transducers were of interest to us in the context of analysis and design. An interest in materials and crystal cuts that would support certain acoustic modes for filter applications led us to solve the Christoffel equations for the allowed propagation conditions similar to the analyses developed by Milsom [Ref. 1] and Hussein and Ristic [Ref. 2]. The condition for allowed modes is that the determinant of the Christoffel equations vanish for a given surface wave velocity, V_s . With this information one could proceed to satisfy the inhomogeneous boundary conditions, in k-space, for a line source. Our intermediate objective was to be able to arrive at the effective permittivity function for an material and crystal orientation specified.

Because of the goal to treat arbitrary crystal orientations, it was necessary to develop or obtain software that would be general enough to express the 4th, 3rd, and 2nd rank tensors (stiffness, piezoelectric, and dielectric tensors, respectively), for any particular crystal cut, in the Christoffel and boundary conditions equations. An existing program called LAYERS [Ref. 3] appeared to fill many of these needs, and it was decided to make use of as much of it as we could.

Our efforts were stymied very early using the LAYERS code because the Christoffel equations did not yield slowness surfaces in agreement with published curves. Qualitatively they were similar; but the magnitude of the deviations were intolerable when compared with the work of Milsom, Wagers, and Ristic [Ref. 2, 4]. There was no way to scale our results to agree with theirs.

Some of our slowness curves appeared to exhibit symptoms of numerical instability and poor convergence. Tolerances were

tightened and loosened to very little avail. We then examined the root-finding code (Muller's inverse parabolic interpolation algorithm) for evaluating the determinant, and convinced ourselves that it was among the very best off-the-shelf codes one could use. It converged rapidly and accurately in actual tests. The Christoffel matrix itself was examined as best we could, considering that rotated tensor expressions were involved. Some unusual scaling was noted in the code but we were unable to ascertain its possible role in generating errors. The project was eventually terminated.

2.2 Power Patterns for SH-Wave IDTs

2.2.1 Analysis

Because of the potential applications of microwave frequency array-steered bulk wave devices, it was decided that the radiation characteristics of shear horizontal (SH) waves should be investigated. One quantity of particular interest that needed to be computed was the far-field power pattern of a planar array of electrodes. The derivation of it is carried out below. Fig. 3 shows, for a double-electrode array and relevant geometry. As several investigators have shown, radiation into an isotropic medium is often a reasonable physical approximation to make, and certainly makes the analysis simpler.

For the double-electrode array shown in Fig. 3 , we note that

$$R = \text{const.}$$

$$\rho = \text{distance from source point to field point} = \left[(R\cos\theta)^2 + (R\sin\theta - x_i)^2 \right]^{1/2} \tag{1}$$

$$x_i = \frac{s}{2} w + i L - \frac{L}{2} \operatorname{sgn}(i) \qquad i = \pm 1, \pm 2, \ldots, \pm \frac{J}{2} \tag{2}$$

$|W| \leq 1$ normalized electrode coordinate

Expanding ρ leads to the following:

$$\rho = \left\{ R^2\cos^2\theta + R^2\sin^2\theta - 2Rx_i\sin\theta + x_i^2 \right\}^{1/2}$$

$$= R\left\{ 1 - 2\sin\theta \left(\frac{s}{2R} W + i\frac{L}{R} - \frac{L}{2R}\,\mathrm{sgn}(i) \right) \right. \tag{3}$$

$$\left. + \left(\frac{s}{2R} W + i\frac{L}{R} - \frac{L}{2R}\,\mathrm{sgn}(i) \right)^2 \right\}^{1/2}$$

For the far-field power distribution, i.e.,

$$\frac{\left| \xi + \frac{I}{2} L - \frac{L}{2} \right|}{R} \ll 1, \tag{4}$$

the quadratic term is negligible by comparison. It follows that

$$\rho = R\left\{ 1 - \sin\theta \left(\frac{s}{2R} W + i\frac{L}{R} - \frac{L}{2R}\,\mathrm{sgn}(i) \right) + \cdots \right\} \tag{5}$$

By far-field we also mean that the half-aperture of the transmitting array is much less than the distance to the observation point at R.

Following Farnell's analysis [Ref.], it is clear that the far-field potential due to all the line sources comprising the array is given by

$$\Phi^{DE}(\theta) = \left(\frac{S}{2}\right) \sum_{\substack{j=-J/2, \\ j\neq 0}}^{J/2} \int_{-1}^{1} dw\, \sigma_j(w)\, H_0^{(1)}[k_t \rho] \qquad (6)$$

where

$k_t = \frac{\omega}{v_t}$ = wavenumber for transversely polarized waves

$$A = \left[\frac{\pi}{2} k_t R\right]^{-1/2} e^{i\left[k_t R - \frac{\pi}{4}\right]} \quad \text{(see below)} \qquad (7)$$

$\sigma_j(w)$ = charge density on j^{th} electrode

$H_0^{(1)}$ = zero-order Hankel function of 1st kind

Using the asymptotic form for the Hankel function gives

$$\Phi^{DE}(\theta) = \frac{S}{2} A \sum_{\substack{j=-J/2, \\ j\neq 0}}^{Jh} e^{-i k_t L \sin\theta \left(j - \mathrm{sgn}(j)/2\right)} \cdot \int_{-1}^{1} dw\, \sigma_j(w) e^{-i k_t \frac{S}{2} w \sin\theta} \qquad (8)$$

Denoting the integral by

$$\hat{\sigma}_j\left[k_t \tfrac{S}{2} \sin\theta\right] = \int_{-1}^{1} dw\, \sigma_j(w) e^{-i k_t \frac{S}{2} w \sin\theta} \qquad (9)$$

and expanding the charge density as usual [Ref.], i.e.,

$$\sigma_j(w) = (1-w^2)^{-\frac{1}{2}} \sum_{n=0}^{N-1} C_n^{(j)} T_n(w) \tag{10}$$

leads to

$$\hat{\sigma}_j(\gamma) = \pi \sum_{n=0}^{N-1} C_n^{(j)} (-i)^n J_n(\gamma) \tag{11}$$

where

$$\gamma \equiv k_t \frac{s}{2} \sin\theta \tag{12}$$

Collecting terms and normalizing $\phi^{DE}(\theta)$ leads to the final expression:

$$\varphi^{DE}(\gamma) = \sum_{j=1}^{J/2} \left\{ \hat{\sigma}_j(\gamma) e^{-i2\frac{\gamma}{2}(j-\frac{1}{2})} + \hat{\sigma}_{-j}(\gamma) e^{i2\frac{\gamma}{2}(j-\frac{1}{2})} \right| \tag{13}$$

where $\varphi^{DE} = \Phi / \frac{S}{2} A$

and

$$\eta = s/L .$$

2.2.2 Results and Discussion

For J = 200, i.e., 100 pairs of electrodes, Fig. shows the far-field power pattern for = 1/2. For an isotropic substrate $\varphi^{DE}(\gamma) = \varphi^{DE}(-\gamma)$. This is not the case for an anisotropic medium, but the difference has been shown to be quite small in many situations by Lewis [Ref. 5]. It is clear that the DE array tuned to its fundemental frequency behaves like an end-five antenna. For these computations the array was assumed to have a periodic polarity impressed on the pairs of electrodes. The infinite array approximation was used in the sense that the expansion coefficients were the same (apart from a sign) for all electrode pairs. The expansions were calculated using N = 6, and the coefficients had the following magnitudes:

$C_0^{(1)} = 0.145814$
$C_1^{(1)} = 0.059185$
$C_2^{(1)} = 0.002699$
$C_3^{(1)} = 0.001402$
$C_4^{(1)} = 0.000047$
$C_5^{(1)} = 0.000031$
$C_6^{(1)} = 0.000001$

Element factors based on calculations and derivations developed above will be determined for both simple and double-electrodes, and will appear in a journal publication.

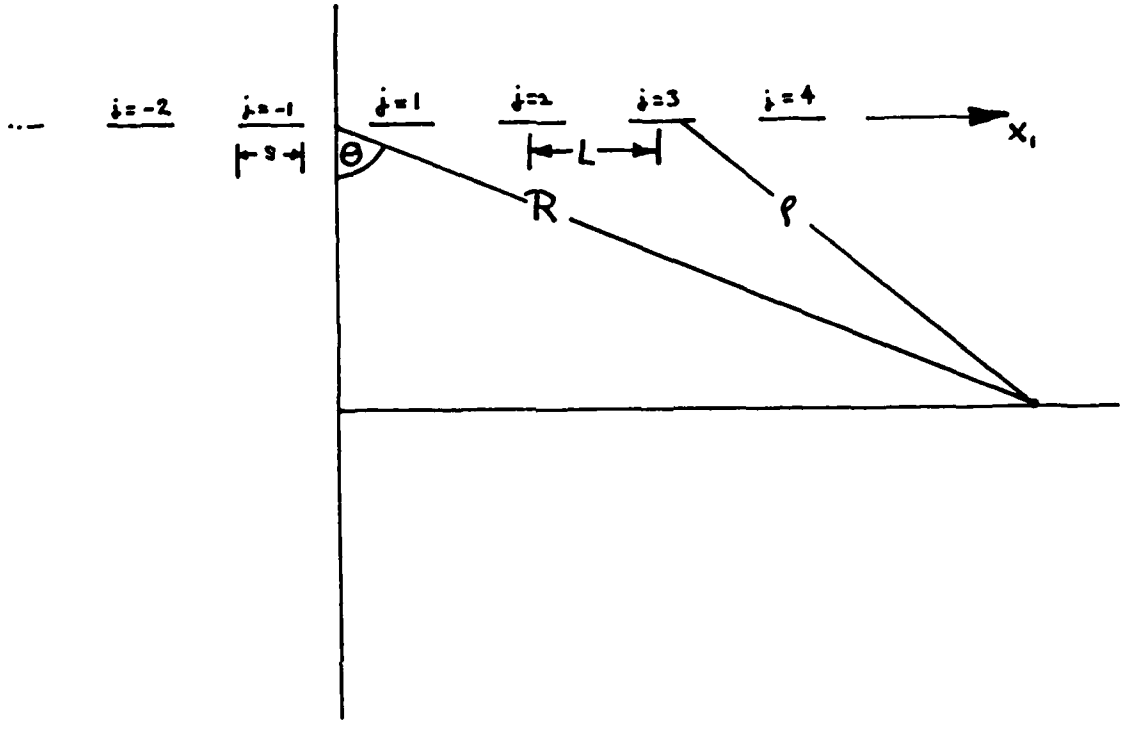

Double-Electrode Array

Figure 3

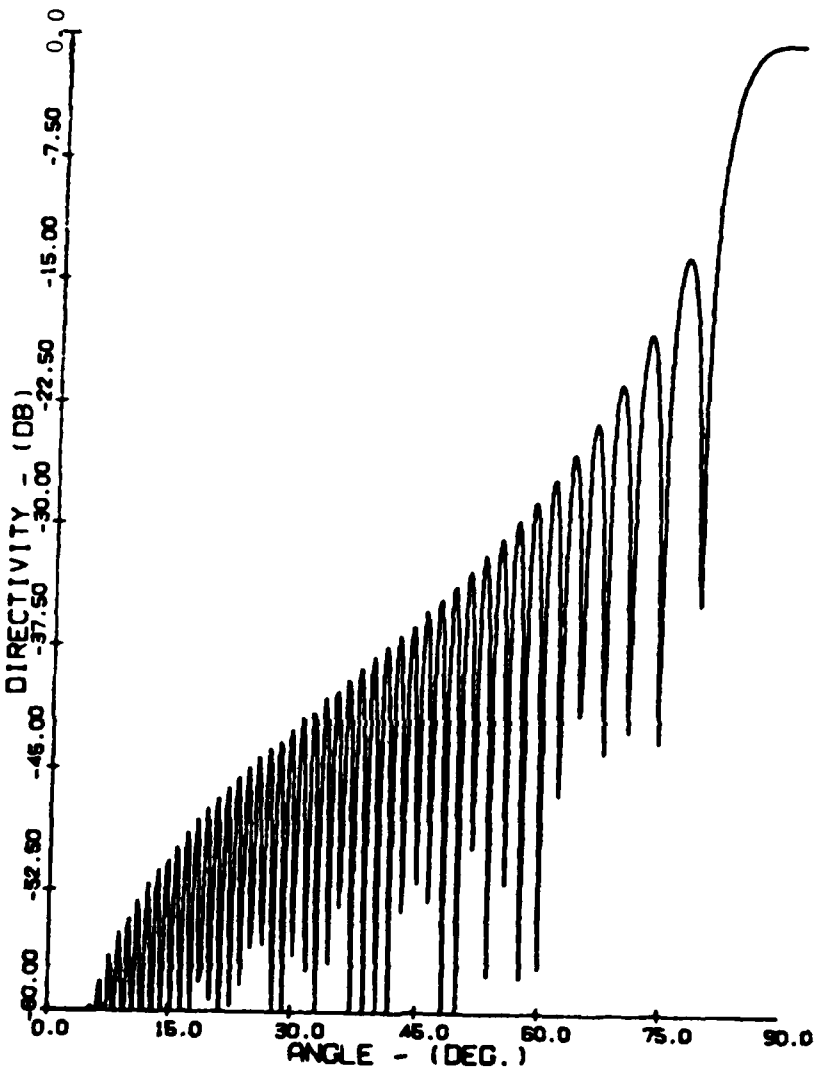

Far-Field Power Pattern

100 Electrode Pairs

Figure 4

REFERENCES

1. R. F. Wilson, N. H. C. Reilly, and M. Redwood, "Analysis of Generation and Detecting of Surface and Bulk Acoustic Waves by Interdigital Transducers", IEEE Trans. Sonics and Ultrasonics, Vol. SU-24, pp. 147-166, 1977.

2. A. M. Hussein and V. M. Ristic, "The Evaluation of the Input Admittance of SAW Interdigital Transducers,"J. Applied Physics, Vol. 50, pp. 4794-4801, July 1979.

3. LAYERS program. This was developed by Hughes Aircraft Corporation for AFGL, 1971.

4. R. Wagers, Physical Acoustics, Vol. XIII, Mason and Thurston, 1977, Ch. 3.

5. W. F. Lewis, "Surface Skimming Bulk Waves", in Proc. 1977 IEEE Ultrasonics Symp., p. 744.

3. Message Identification

A low-frequency method of communication was tested between Forestport, New York and Troy, New Hampshire. This method involved the transmission, reception and subsequent analysis of time-delayed low-frequency groundwaves (25 KHz) which were digitized and stored on magnetic tape. The analysis, detailed below, included determining the time-delay of the groundwave in each record. A message was encoded by varying the time-delay of a number of consecutive records wherein each delay corresponded to certain alphabetic character.

A computer program was designed to perform correlations between a standard waveform and that of each record on tape by mathematically shifting the former along the latter to determine the position of maximum correlation. This point represents the time-delay of the given waveform.

A well-known cross-correlation function

$$r(K) = \frac{\sum_{t=1}^{n-K} x_t y_t + \bar{y}\sum_{t=n+1-K}^{n} x_t + \bar{x}\sum_{t=1}^{K} y_t - (n+K)\bar{x}\bar{y}}{\left[\sum_{t=1}^{n} x_t^2 - n\bar{x}^2 \sum_{t=1}^{n} y_t^2 - n\bar{y}^2\right]^{1/2}} \qquad (1)$$

was used in which x and y are the values of the standard waveform and the one being tested, n, is the total number of elements in each waveform and k is the particular shift of the standard along the waveform being compared.

The field tapes consisted of records of length 256; each representing a time-frame of the same number of microseconds and

each containing one waveform 40 microseconds long. Blocks of 22 records were created by transmitting 22 consecutive waveforms with the same time-delay. Many tapes containing waveforms of varying signal strengths were created for later analysis.

Initial results, comparing the standard waveform to those of a tape of high signal-to-noise ratio were successful, i.e., the message was easily decoded. There were problems, however, decoding tapes having low S/N ratios. Averaging five consecutive records before cross-correlating was tried but since there is no physical indicator of the beginning of a given block, it was impossible to be sure whether one was averaging records in the same block (same time-delays) or those in two different blocks. Understandably, averaging records in two different blocks would tend to worsen results since an additional waveform would be introduced into the averaged record and this was found to be the case.

It was determined that more advanced signal processing techniques are necessary to improve the S/N ratio prior to applying the cross-correlation method. Current investigations include the use of fast Fourier transforms and filtering to eliminate noise and improve the S/N ratio.

4. Nonlinear Transcendental Equations

Our objective was to solve a system of 5 nonlinear transcendental equations. The first 3 pertained to the reflection of an incident ray from a flat facet having a slope angle β and an orientation angle α with respect to the transmitter-receiver line of sight. The last two equations ensured that the reflected ray arrived at the receiver if the height of the point of reflection was required to be H and the distance between the transmitter and the receiver, D.

An attempt to solve the equations analytically failed. The next effort was to obtain an approximate solution of the system of equations. The system was transformed through several substitutions into a system of algebraic equations with the hope of diminishing the computer time demands, because it was known that searching for the solution using an iterative process would be computationally expensive, especially when there was no information for good starting values. A rapidly converging iterative process was applied to the algebraic system; the subroutine ZCNT from the IMSL library was used. However, it turned out to take considerable computer time, 2000 sec. For this reason, the paper from which these equations were derived was reexamined and found to have a misprint. A careful examination of the geometry showed the equations weren't necessary at all for the determination of the directions (ϑ, θ) of the incident ray and directions (μ, ν) of the reflected ray. All unknown angles could be found directly from the geometry of the reflection by solving simple solid geomtery problems.

The new calculations took less than 1 second of computer time, and the results had obvious geometrical meaning. Plots were made of $\nu(\mu)$ for different values of the parameters.

5. Tropospheric Range Error Correction Utilizing Exoatmospheric Sources

5.1 Introduction

Tropospheric refractive range and angle errors limit the performance of radar and navigation systems that operate at low elevation angles. For some locations and for many applications, antenna pointing corrections based on surface refractivity alone or, if necessary, a vertical refractivity profile are adequate. However, new systems that operate at very low elevation angles require improved accuracy. More accurate angle error corrections can be obtained by utilizing calibration sources (such as the limb of the sun, radio sources, satellites) the angular positions of which are precisely known to a sufficient accuracy--the range error correction is still a problem. It has been shown that it is possible to develop a method for obtaining an improved range error correction by utilizing measured angle error data for the same ray path. An expression for the refractive angle correction for a target, based on the measured angle error of the calibration source is first derived (1).

Both the target and calibration source are assumed to be outside the troposphere where the index of refraction $n(r)$ is approximately unity, hence the angular refraction γ is the same for both

$$\sin(\gamma-\epsilon_1)\left[\sqrt{(a+h_1)^2-a^2\cos^2(\theta_a-\epsilon_1)}-a\sin(\theta_a-\epsilon_1)\right]$$

$$=\sin(\gamma-\epsilon_2)\left[\sqrt{(a+h_2)^2-a^2\cos^2(\theta_a-\epsilon_2)}-a\sin(\theta_a-\epsilon_2)\right] \quad (1)$$

In this equation, ϵ_2 , the angle error of the calibration source, and the initial elevation angle of antenna are known, as are approximate heights h_1 and h_2 of the target and calibration source (see Fig. 5).

There is a direct formula to express the angle error corrections ϵ_1 , ϵ_2 (for the target or for the calibration source respectively) through the angular refraction .

$$\epsilon_i = \tan^{-1}\left\{ \frac{\cos\tau - \sin\tau \cdot \tan\theta_i - n(r_i)/n_a}{n(r_i)/n_a \cdot \tan\theta_a - \sin\tau - \cos\tau \cdot \tan\theta_i} \right\} \qquad (2)$$

where

$$n(r_i) = 1$$

and

$$\theta_i = \frac{a n_a \cos\theta_a}{r_i}$$

under assumptions mentioned above.

However, before the angle error of the target ϵ_1 can be determined, the angular refraction τ must be found

$$\tau = \frac{\pi}{2} + \epsilon_2 - \cos^{-1}\left[\frac{a}{a+h_2} n_a \cos\theta_a\right] - \sin^{-1}\left[\frac{a}{a+h_2}\cos(\theta_a - \epsilon_2)\right] \quad (3)\ *$$

The angular position of calibration sources are precisely known, so it is possible to calculate the angle correction ϵ_2 by taking the difference of the apparent position θ_a which is measured and the true position which is tabulated:

$$\epsilon_2 = \theta_a - \beta_2 . \quad (4)$$

---

*It should be emphasized that the following formula is correct as well.

$$\tau = \pi/2 + \epsilon_2 - \cos^{-1}\left[\frac{a}{a+h_1} n_a \cos\theta_a\right] - \sin^{-1}\left[\frac{a}{a+h_1}\cos(\theta_a - \epsilon_1)\right] \quad (3')$$

since the angular refraction τ for the target is the same. Then with τ known from (3) the angle error of the target ϵ_1 can be calculated from (1).

It is then shown that the range error correction for a target can be expressed as a function (integral) of the angular refraction. The angle error for the target ϵ_1 is also involved. Therefore, the range error correction can be calculated from a set of angle error measurements (4).

The range error $\Delta Re\ (a,\ C_a,\ r_1)$ correction is defined by

$$\Delta R_e(a, C_a, r_1) = R_e(a, C_a, r_1) - R_o(a, C_a, r_1) \qquad (5)$$

where R_e and R_o are the apparent (or radio) range and the true (or slant) range respectively.

The expression for calculating the range error correction is given by

$$\Delta R_e(a, C_a, r_1)\Big|_{C_a=C}^{C_a} = \Big\{ \sqrt{(a+h_1)^2 - (an_a C_a)^2} \qquad (6)$$

$$- \sqrt{(a+h_1)^2 - a^2 [C_a C_{ra}\epsilon_1 + (1-C_a^2)^{1/2} \sin\epsilon_1]^2}$$

$$- a\,[C_a \sin\epsilon_1 + (n_a - C_{ra}\epsilon_1)(1-C_a^2)^{1/2}]\Big\}\Big|_{C_a=C}^{C_a}$$

$$+ an_a\,[C_a \tau(a, C_a, r_1) - C\tau(a, C, r_1)] - an_a \int_C^{C_a} \tau(a, C_a, r_1)\, dC_a$$

with following denotations:

C_a - is $\cos(\theta_a)$, where θ_a - the elevation angle of the antenna;

C - is $\cos(\theta)$, where θ the elevation angle of the calibration source;

a - the distance of the antenna from the center of the earth;

$a+h_1 = r_1$ - the distance of the target from the center of the earth;

n_a - the quotient $(a + h_1)/a$;

ϵ_1 - the angle error of the target;

$\tau(a, C_a, r_1)$ - is the total angular refraction along the ray path (the ray path lies in the great circle plane, determined by the locations of the antenna and target, see Fig. 1).

$$\tau(a, C_a, r_1) = -a n_a C_a \int_a^{r_1} \frac{n'\, dr}{n\sqrt{(rn)^2 - (a n_a C_a)^2}} \qquad (7)$$

The function n(r) is expressed as follows:

$$n(r) = 1 + N(r-a) * 10^{-6},$$

$$N(r-a) = \begin{cases} N_s + \Delta N * (r-a) & 0 \leq r-a \leq 1 \\ N_1 \exp[-c(r-a)] & 1 \leq r-a \leq q \\ 105 \exp[-0.1424(r-a-q)] & q \leq r-a \end{cases}$$

here

$$N_s = 313.0$$

$$\Delta N = -7.32 \exp(0.005577 N_s)$$

$$N_1 = N_s + \Delta N$$

$$C = \frac{1}{\epsilon} \ln(N_1/105)$$

This formula for N(r-a) corresponds to "Modified Effective Earth's Radius Model" which is usually used to solve refraction problems.

It should be emphasized that (6) provides the difference in range error for elevation angles corresponding to the limits C_a and C. For example, for the case of the sun as a calibration source, it is the difference of range errors for C and C_a corresponding to elevation angles of 60 and C_a, respectively.

In order to obtain the total range error for an elevation angle C_a (with $\theta_a \leq 5°$) it is necessary to estimate the total range error for an angle of $60°$. This is not considered a serious limitation since the angular refraction for very high angles is minimal; also, the corresponding range error is relatively small.

5.2 Task Description

The problem to analyze consisted of the following steps:

1) to select the numerical integration technique which provides the least number of measurements required to guarant · a given accuracy of integration for the integral

$$\int_{C}^{C_a} \tau(a, C_a, r_1)\, dC_a \qquad (8)$$

2) to analyze the sensitivity of this integral to the small perturbation of θ values (the measurement errors).

3) to analyze the sensitivity of the angle error ϵ_1 to the small perturbations of θ values (the measurement errors).

4) to analyze the sensitivity of the range error correction $\Delta R_e|^c$ to the small perturbations of θ values. Values of β in expression (3) are supposed to be exact, so

$$\Delta\epsilon_2 = \Delta\theta_a.$$

To obtain the range error correction from (6) the following procedure was suggesed:

1) Select a set of elevation angles between θ_a and θ and obtain the corresponding set of the angle errors of the calibration source, utilizing the relation (4). Elevation angles θ are to be measured, the appropriate true angular positions β of the calibration source are to be found from tables (if, for example, the sun is the calibration source, the solar ephemeris is to be utilized).

2) Calculate the appropriate angular refractions τ for the selected set of elevation angles from the relation (3).

3) Calculate the angle error ϵ_1 from the equation (1). For this calculation only one measurement is needed.

4) Use the obtained set of τ values for the approximate numerical calculation of the integral on the right side of the expression (6).

The accuracy of this technique is dependent on many factors. Especially, of primary importance are the accuracy with which the angle error can be measured, the refractivity structure of the troposphere and the number of angle error measurements.

Of secondary importance are the accuracy of the heights and angular coordinates of the calibration sources, the height of the target, the measurement of the surface index of refraction , the numerical integration techniques that are employed, and the estimate of the total range error contribution from the angular refraction at elevation angles above the maximum elevation angle of calibration sources.

5.3 Work Description

1) A numerical experiment was designed to select the appropriate numerical integration technique which would guarantee a given accuracy with the least number of nodes , i.e., that would use the least number of required measurements. The exact theoretical expression for the angular refractivity

$$\tau(a, C_a, r_1) = -a n_a C_a \int_a^{r_1} \frac{n'(r)\, dr}{n(r)\sqrt{[r n(r)]^2 - [a n_a C_a]^2}} \qquad (9)$$

was utilized in this experiment.

It should be emphasized that this integral is close to an integral with a singularity when $\theta_a \to 0$.

The relative accuracy of calculations considered to be equal to $0.5 * 10^{-3}$; there was no reason to consider higher accuracies since the value a, the antenna distance from the center of

the earth, had no more than 3 correct significant digits. Three methods for numerical integration were compared: Romberg rule, Simpson formula and Hermite formula, the nodes being selected automatically. It turned out that Simpson's method gave noticable better results; for example:

θ_a	Number of Nodes		
	Simpson Rule	Romberg Rule	
3°	25	41	$\theta = 20°$
0..01°	53	73	

The nodes selected by Simpson's method were utilized for calculation of the integral (8), but the angular refractivity was computed from the expression (3) with the appropriate interpolation along the table. Results of two different ways of the calculation of the integral (8) coincided with 3 significant digits. Therefore, the set of angles obtained from the first preliminary calculation utilizing the expression (9) for the angular refractivity can be used as the set of measurement angles.

2) The sensitivity of the integral (8) to perturbations was checked numerically. Three significant digits of the integral remained unchanged while perturbations didn't exceed $0.5 * 10^{-3}$ in absolute values. Such precise measurement

can be accomplished practically, so the sensitivity is suitably low.

3) The sensitivity of angle error ϵ_1 with respect to perturbation of angle error ϵ_2 of the calibration source, (under assumption that β_2, a_2, h_2 are exact), has been checked numerically. It turned out that

$$|\delta\epsilon_1| \leq 2\,|\delta\epsilon_2|$$

when angles θ_a belong to the interval $0^\circ \leq \theta_a \leq 5^\circ$.

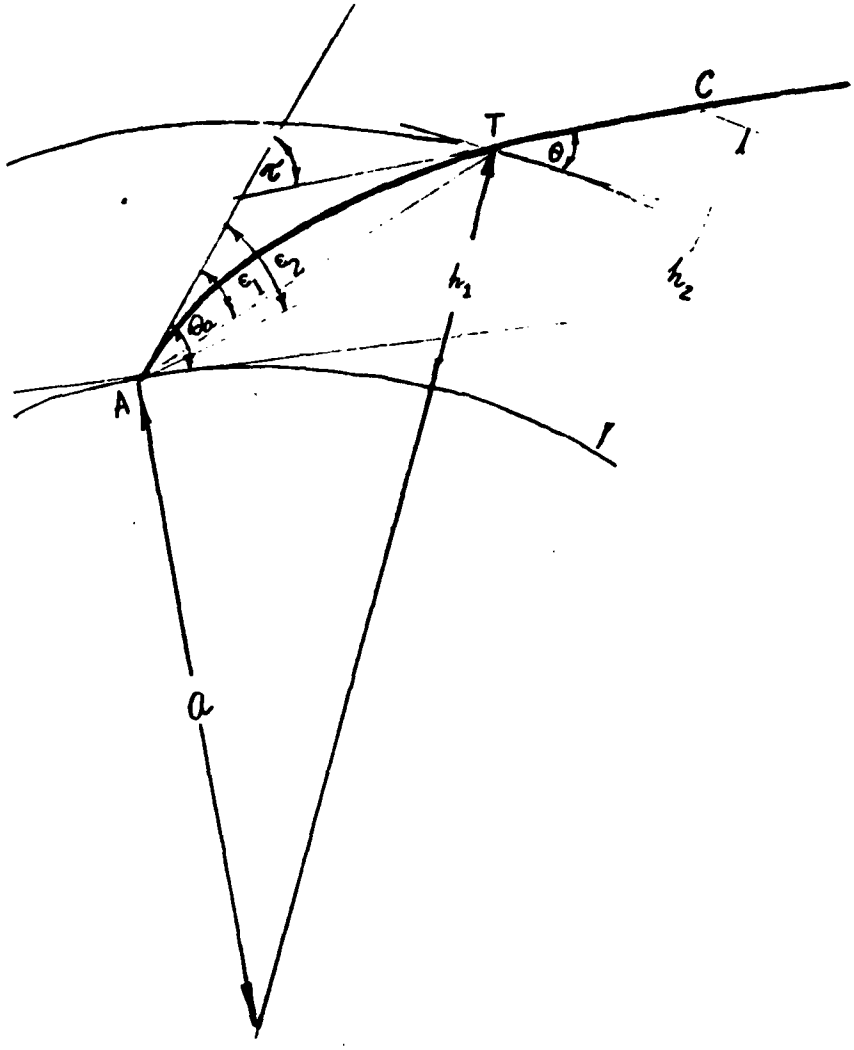

Geometry of Interest

Figure 5

References

1. K. Mann and E. E. Altshuler, "Tropospheric refractive angle and range error corrections utilizing exoatmospheric sources", *Radio Science*, Vol. 16, Number 2, March-April, 1981.

6. Maximum Signal Power at a Critical Down-Range Distance

6.1 Introduction

Over-the-horizon (OTH) radar signals are reflected from several layers of the ionosphere before illuminating some point of the earth. The optimum frequency f and launch angle β to be utilized may be predicted via ray-tracing techniques. The goal of the program PWRMAX is to determine f and β for maximum signal power at a critical down-range r_c . Both maximums were needed; the local maximum of power and absolute maximum of power.

In order to reach this goal the program PWRMAX combines a high-speed ray-tracing computer code with a power versus range r curve-fitting algorithm.

6.2 General Discussion

The search for the optimum frequency is performed over the initial intervals of frequencies $[F_1 , F_2]$ and angles $[B_1 , B_2]$, the intervals being determined from physical considerations.

The ray-tracing computer code allows one to obtain the corresponding values of power p and range r for each pair

$$(f, \beta) \in [F_1 , F_2] \otimes [B_1 , B_2].$$

For each fixed frequency $f_i \in [F_1, F_2]$ $(i = 1,2,\ldots,N)$ and variable $\beta_{ij} \in [B_1, B_2]$ $(j = 1,2,\ldots,M)$ a table of "power p_{ij} " versus "range r_{ij} " may be obtained:

$f = f_i$				
β_{i1}	β_{i2}	β_{i3}	. . .	β_{iM}
r_{i1}	r_{i2}	r_{i3}	. . .	r_{iM}
p_{i1}	p_{i2}	p_{i3}	. . .	p_{iM}

Such tables represent functional dependencies of "power" versus "range" and must be examined at the beginning.

The functional dependencies may be described approximately by the quadratic obtained using standard least squares. Denoting the appropriate polynomial by $\hat{P}_i(r)$, the following approximate equality is correct:

$$P_i(r) \approx \hat{P}_i(r) \qquad (1)$$

The value of power at the point r_c may be approximately calculated as $P_i(r_c)$:

$$P_i(r_c) \approx \hat{P}_i(r_c) \qquad (2)$$

This leads to a table of the form

f_1	f_2	. . .	f_N
$\hat{P}_1(r_c)$	$\hat{P}_2(r_c)$	. . .	$\hat{P}_N(r_c)$

which may be treated as an approximate representation of the functional dependence $P_c(f)$ "the value of power at the

down-range r_c " versus "frequency". Using the functional form of the above table, the absolute maximum may be obtained with standard methods (involving either simple selection of the least square curve fitting with further selection of absolute maximum for a parabola.

With regard to the local maximum of power, the least squares curve-fitting usually is not a suitable method to investigate local properties of fitted curves. But if certain conditions apply, the fitting curve may be used for approximate calculations of the local maximum.

Functional dependencies $P_i(r)$ $(i=1,2,\dots,N)$ were assumed to be quite smooth and to have the single local maximum in the neighborhood of the point r_c. This assumption was justified physically and with numerical experiments.

If a curve $P_i(r)$ is shaped as assumed, the coordinates $(\hat{r}_i^{max}, \hat{P}_i^{max})$ of the fitting parabola $\hat{P}_i(r)$ local maximum may be regarded as an approximation to the coordinates (r_i^{max}, P_i^{max}) of the local maximum of $P_i(r)$. The functional dependency "frequency" versus "range-coordinate of local maximum", $F_{l_{max}}(r)$ may then be approximately restored using standard least square so that

$$F_{l_{max}}(r) \approx \hat{F}_{l_{max}}(r) \qquad (3)$$

where $F_{l_{max}}(r)$ is a polynomial of second degree.

Finally, the frequency that provides the local maximum of power at the point r_c may be calculated approximately as

$$f_{opt.} \approx \hat{F}_{l_{max}}(r_c) \qquad (4)$$

7. Multi-Hop Propagation

7.1 Introduction

The computation of the number of hops versus launch angle for geometric multi-hop propagation between concentric boundaries presents certain analytical problems.

This problem is mainly due to the implicit form in which relations between number of hops, launch angle, relative transmission delay, distance and height of transmission boundary are presented.

To obtain iso-height and transmission-delay contours, explicit formulas for number of hops and launch angle of the ray were derived.

This representation also obviates the separate treatment of multi-hop round-the-world propogation as an additional case to the propagation over a certain distance along the surface of earth.

7.2 Analysis of Parametric Equations

For mirror reflections between concentric spherical ionosphere and earth over a distance (d) along the surface of earth the following parametric equations apply for the height of reflection boundary (h) and relative transmission-delay (δ)

$$h = R \sin\left(\frac{d}{2nR}\right) \tan\left(\theta + \frac{d}{2nR}\right) - R\left(1 - \cos\left(\frac{d}{2nR}\right)\right) \quad (1)$$

$$\delta_d = \frac{2nR}{c} \sin\left(\frac{d}{2nR}\right) \sec\left(\theta + \frac{d}{2nR}\right) - \frac{d}{c} \quad (2)$$

where R is radius of earth, θ is launch angle of the ray, n is number of hops and c is velocity of light.

In addition, the round-the-world case is presented by equations

$$\delta_{2\pi R} = \frac{2R}{c}\left\{ n\sqrt{1 - \frac{\cos\theta}{\cos(\theta+\frac{\pi}{n})}\left[2\cos(\frac{\pi}{n}) - \frac{\cos\theta}{\cos(\theta+\frac{\pi}{n})}\right]} - \pi \right\} \quad (3)$$

$$h = R\left[\frac{\cos\theta}{\cos(\theta+\frac{\pi}{n})} - 1\right] \quad (4)$$

An analysis of given parametric equations yields a unique set of formulas for launch angle (θ) and number of hops (h).

$$n = \frac{c}{2R}\left(\delta_1 + \frac{d}{c}\right)\left[\cos\theta \cdot \operatorname{ctg}\frac{d}{2nR} - \sin\theta\right]$$

$$= B \pm \frac{\left[B^2 - \left(1 - \frac{n}{A^2}\right)\left(B^2 - \frac{n^2}{A^2}\right)\right]^{1/2}}{1 - \frac{n^2}{A^2}} \quad (5)$$

where

$$A = \frac{c\delta_d + d}{2R} \tag{6}$$

$$B = ct_g \frac{d}{2\pi R} \tag{7}$$

Thus, the round-the-world case could be derived easily by substituting distance d with $2\pi R$ and iso-height and transmission delay contours could be easily obtained.

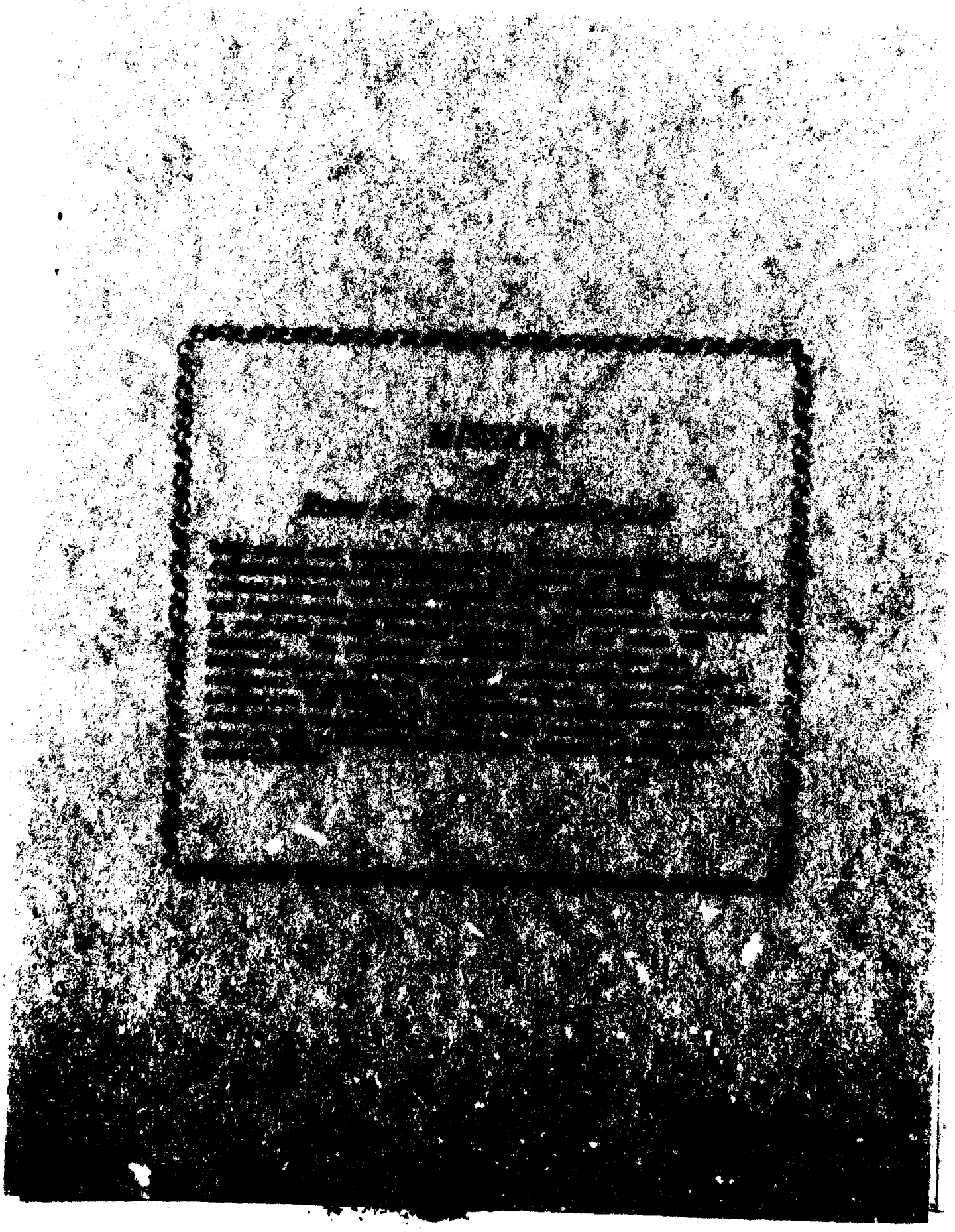

END

DATE
FILMED

3-82

DTIC